SUPPLEMENTARY MATERIALS

Controlling Achiral and Chiral Properties with an Electric Field: A Next Generation QTAIM Interpretation

Wenjing Yu[1], Zi Li[1], Yuting Peng, Feng Xinxin, Tianlv Xu[1], Herbert Früchtl[2], Tanja van Mourik[2], Steven R. Kirk[*1] and Samantha Jenkins[*1]

[1]Key Laboratory of Chemical Biology and Traditional Chinese Medicine Research and Key Laboratory of Resource National and Local Joint Engineering Laboratory for New Petro-chemical Materials and Fine Utilization of Resources, College of Chemistry and Chemical Engineering, Hunan Normal University, Changsha, Hunan 410081, China

[2]EaStCHEM School of Chemistry, University of Saint Andrews, North Haugh, St Andrews, Fife KY16 9ST, Scotland, United Kingdom.

email: steven.kirk@cantab.net
email: samanthajsuman@gmail.com

1. Supplementary Materials S1. NG-QTAIM and stress tensor theoretical background and procedure to generate the stress tensor trajectories $\mathbb{T}_\sigma(s)$.

2. Supplementary Materials S2. Distance measures for alanine with and without an applied electric field.

3. Supplementary Materials S3. Scalar measures with for alanine with and without an applied electric field.

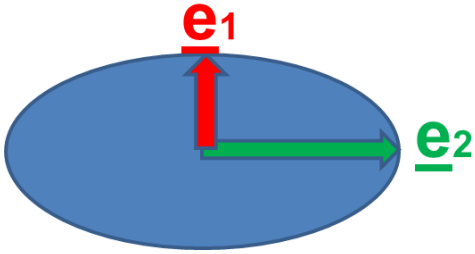
4. Supplementary Materials S4. Additional $\mathbb{T}_\sigma(s)$ and tables of the alanine torsional C1-C2 *BCPs.*

1. Supplementary Materials S1.

I(i) *QTAIM and stress tensor bond critical point (BCP) properties; ellipticity ε:*

The four types of QTAIM critical points are labeled using the notation (R, ω) where R is the rank of the Hessian matrix, i.e., the number of distinct non-zero eigenvalues and ω is the signature (the algebraic sum of the signs of the eigenvalues); the (3, -3) [nuclear critical point (*NCP*), a local maximum], (3, -1) and (3, 1) [saddle points, referred to as bond critical points (*BCP*) and ring critical points (*RCP*), respectively] and (3, 3) [the cage critical points (*CCP*)]. In the limit that the forces on the nuclei are zero, an atomic interaction line[Bader, R. F. W. A Bond Path: A Universal Indicator of Bonded Interactions. *J. Phys. Chem. A* **102**, 7314–7323 (1998)], the line passing through a *BCP* and terminating on two nuclear attractors along which the charge density $\rho(\mathbf{r})$ is locally maximal with respect to nearby lines, becomes a bond-path [Bader, R. F. W. Bond Paths Are Not Chemical Bonds. *J. Phys. Chem. A* **113**, 10391–10396 (2009)]. The full set of critical points with the bond-paths of a molecule or cluster is referred to as the molecular graph.

- Ellipticity $\varepsilon = |\lambda_1|/|\lambda_2| - 1$.



Scheme S1. The cross section through a bond at the bond critical point (*BCP*). The λ_1 and λ_2 eigenvalues with associated eigenvectors $\underline{\mathbf{e}}_1$ and $\underline{\mathbf{e}}_2$ respectively, define the axes of the ellipse and indicate the magnitudes of the least and greatest extents of the distribution of $\rho(\mathbf{r})$.

The ellipticity, ε, defined as $\varepsilon = |\lambda_1|/|\lambda_2| - 1$, quantifies the relative accumulation of the electronic charge density $\rho(\mathbf{r_b})$ distribution in the two directions $\underline{\mathbf{e}}_1$ and $\underline{\mathbf{e}}_2$ that are perpendicular to the bond-path at a Bond Critical Point (*BCP*) with position $\mathbf{r_b}$. For ellipticity $\varepsilon > 0$, the shortest and longest axes of the elliptical distribution of $\rho(\mathbf{r_b})$ are associated with the λ_1 and λ_2 eigenvalues, respectively. From the electron-preceding perspective a change in the electronic charge density distribution that defines a chemical bond causes in a change in atomic positions [*J. Am. Chem. Soc.* **96**, 24–30(1974)]. Bone and Bader later proposed that the direction of motion of the atoms that results from a slightly perturbed structure coincides with the direction of motion of the electrons [*J. Phys. Chem.* **100**, 10892–10911(1996)]; this was later confirmed [*J. Phys. Condens. Matter* **12**, 10325–10333(2000)] [*J. Chem. Phys.* **130**, 154104-154104–11(2009)].

I(ii). *QTAIM bond-path properties; bond-path length (BPL), bond-path curvature, stress tensor eigenvalue $\lambda_{3\sigma}$ and the stress tensor trajectory $\mathbb{T}_\sigma(s)$:*

The bond-path length (BPL) is defined as the length of the path traced out by the $\underline{\mathbf{e}}_3$ eigenvector of the

Hessian of the total charge density $\rho(\mathbf{r})$, passing through the *BCP*, along which $\rho(\mathbf{r})$ is locally maximal with respect to any neighboring paths. The bond-path curvature separating two bonded nuclei is defined as the dimensionless ratio (BPL - GBL)/GBL, where the BPL is defined to be the bond-path length associated and GBL is the inter-nuclear separation. The BPL often exceeds the GBL particularly in strained bonding environments [Jenkins, S. & Heggie, M. I. Quantitative analysis of bonding in 90° partial dislocation in diamond. *J. Phys. Condens. Matter* **12**, 10325 (2000)]. Earlier, one of the current authors hypothesized that a bond-path may possess 1-D, 2-D or a 3-D morphology [*Chem. Phys. Lett.* **317,** 97–102 (2000)], with 2-D or a 3-D bond-paths associated with a *BCP* with ellipticity $\varepsilon > 0$, being due to the differing degrees of charge density accumulation, of the λ_2 and λ_1 eigenvalues respectively. Bond-paths possessing zero and non-zero values of the bond-path curvature defined by equation **(2)** can be considered to possess 1-D and 2-D topologies respectively. We start by choosing the length traced out in 3-D by the path swept by the tips of the scaled $\underline{\mathbf{e}}_2$ eigenvectors of the λ_2 eigenvalue, the scaling factor being chosen as the ellipticity ε, see **Scheme S1 (a)**.

- Stress tensor eigenvalue $\lambda_{3\sigma}$

This is used as a measure of bond-path instability, for values of $\lambda_{3\sigma} < 0$ and is calculated within the QTAIM partitioning.

The quantum stress tensor $\boldsymbol{\sigma}(\mathbf{r})$ is directly related to the Ehrenfest force by the virial theorem and therefore provides a physical explanation of the low frequency normal modes that accompany structural rearrangements [*Int. J. Quantum Chem.* **115,** 1678–1690 (2015).]. In this work we use the definition of the stress tensor proposed by Bader to investigate the stress tensor properties within QTAIM. [*J. Chem. Phys.* **73,** 2871–2883 (1980).]. The quantum stress tensor $\boldsymbol{\sigma}(\mathbf{r})$ is used to characterize the mechanics of the forces acting on the electron density distribution in open systems, defined as:

$$\boldsymbol{\sigma}(\mathbf{r}) = -\frac{1}{4}\left[\left(\frac{\partial^2}{\partial \mathbf{r}_i \partial \mathbf{r}'_j} + \frac{\partial^2}{\partial \mathbf{r}'_i \partial \mathbf{r}_j} - \frac{\partial^2}{\partial \mathbf{r}_i \partial \mathbf{r}_j} - \frac{\partial^2}{\partial \mathbf{r}'_i \partial \mathbf{r}'_j}\right) \cdot \gamma(\mathbf{r}, \mathbf{r}')\right]_{\mathbf{r}=\mathbf{r}'} \qquad \textbf{(2)}$$

Where $\gamma(\mathbf{r},\mathbf{r}')$ is the one-body density matrix,

$$\gamma(\mathbf{r}, \mathbf{r}') = N \int \Psi(\mathbf{r}, \mathbf{r}_2, \ldots, \mathbf{r}_N)\Psi^*(\mathbf{r}', \mathbf{r}_2, \ldots, \mathbf{r}_N)\mathrm{d}\mathbf{r}_2 \cdots \mathrm{d}\mathbf{r}_N \qquad \textbf{(3)}$$

The stress tensor is then any quantity $\boldsymbol{\sigma}(\mathbf{r})$, that satisfies equation **(2)** since one can add any divergence free tensor to the stress tensor without violating this definition [*J. Phys. Chem. A*, 2010, **114**, 8884–8895.], [*J. Phys. Chem. A*, 2011, **115**, 13001–13006.] [*J. Chem. Phys.*, 1980, **73**, 2871–2883.].

Earlier, it was found that the stress tensor trajectories $\mathbb{T}_\sigma(s)$ were in line with physical intuition [*Chem. Phys. Lett.* **667,** 25–31 (2017)].

If we first consider a tiny cube of fluid flowing in 3-D space the stress $\Pi(x, y, z, t)$, a rank-3 tensor field, has nine components [*Interdiscip. Appl. Math.* xxii,405 (2006).] of these the three diagonal components Π_{xx}, Π_{yy}, and Π_{zz} correspond to normal stress. A negative value for these normal components signifies a compression of the cube, conversely a positive value refers to pulling or tension, where more negative/positive values correspond to increased compression/tension of the cube. Diagonalization of the stress tensor $\boldsymbol{\sigma}(\mathbf{r})$, returns the principal electronic stresses Π_{xx}, Π_{yy}, and Π_{zz} that are realized as the stress tensor eigenvalues $\lambda_{1\sigma}$, $\lambda_{2\sigma}$, $\lambda_{3\sigma}$, with corresponding eigenvectors $\underline{\mathbf{e}}_{1\sigma}$, $\underline{\mathbf{e}}_{2\sigma}$, $\underline{\mathbf{e}}_{3\sigma}$ are calculated within the QTAIM partitioning.
Previously, $\lambda_{3\sigma}$ was used to detect the lowering of the symmetry, caused by a torsion about the central C-C bond in biphenyl, inducing a phase transition [*Int. J. Quantum Chem.* **115,** 1678–1690 (2015)]. The *BCP*s calculated with QTAIM and stress tensor partitionings will not always coincide, particularly under the application of external force, such as an applied torsion.

I(iii). *The stress tensor trajectory $\mathbb{T}_\sigma(s)$ background, interpretation and numerical procedures to generate:*

The changing orientation and characteristics will be undertaken using the stress tensor trajectory space formalism of the bond critical points (*BCP*s). The stress tensor trajectory $\mathbb{T}_\sigma(s)$ space $\mathbb{U}_\sigma$ has been previously used to track changing orientation and characteristics of the series of rotational isomers of the S and R stereoisomers of the lactic acid [*Journal of the American Chemical Society*, **141**(13), 5497–5503 (2019)], the prediction of torquoselectivity in competitive ring-opening reactions [*J. Comput. Chem.* **37,** 2722–2733 (2016)], elucidating the mechanism of photochromism and fatigue switches [*Int. J. Quantum Chem.* **118**(13), e25565 (2018)], the functioning of doped azophenine switches [*Intl. J. Quantum. Chem.* **118**(16), e25676 (2018)] as well as for the reaction pathways of $(H_2O)_5$ [*Chem. Phys. Lett.* **667,** 25–31 (2017)]. The stress tensor trajectory $\mathbb{T}_\sigma(s)$ is intended for use in applications where there will be a finite, i.e. non-zero translation of a given *BCP*, either in real space or the stress tensor trajectory $\mathbb{T}_\sigma(s)$ space $\mathbb{U}_\sigma$. For instance, previously, we examined torsion about the *BCP* located at the fixed 'pivot' of the torsion of the C-C bond linking the two phenyl rings in biphenyl where, as expected, was no significant translation of the central *BCP* [*Int. J. Quantum Chem.* **115,** 1678–1690 (2015)].
For a given *BCP*, the stress tensor eigenvectors $\{\underline{\mathbf{e}}_{1\sigma}, \underline{\mathbf{e}}_{2\sigma}, \underline{\mathbf{e}}_{3\sigma}\}$ for that *BCP* at the step of the normal mode displacement are used as the projection set for the entire stress tensor trajectory $\mathbb{T}_\sigma(s)$. The location in the stress tensor $\mathbb{U}_\sigma$-space $\mathbf{dr}'(s)$ corresponding to the direction vector $\mathbf{dr}(s)$ in real space is given by $\{(\underline{\mathbf{e}}_{1\sigma}\cdot\mathbf{dr}), (\underline{\mathbf{e}}_{2\sigma}\cdot\mathbf{dr}), (\underline{\mathbf{e}}_{3\sigma}\cdot\mathbf{dr})\}$. The location in the $\mathbb{U}$-space $\mathbf{dr}'(s)$ corresponding to the direction vector $\mathbf{dr}(s)$ in real space is given by $\{(\underline{\mathbf{e}}_1\cdot\mathbf{dr}), (\underline{\mathbf{e}}_2\cdot\mathbf{dr}), (\underline{\mathbf{e}}_3\cdot\mathbf{dr})\}$.

The explanation and numerical procedures for the stress tensor $\mathbb{T}_\sigma(s)$ trajectories.

The stress tensor trajectory $\mathbb{T}_\sigma(s)$ is constructed exclusively using the frame of reference defined by the eigenvectors $\{\pm\underline{\mathbf{e}}_{1\sigma},\pm\underline{\mathbf{e}}_{2\sigma},\pm\underline{\mathbf{e}}_{3\sigma}\}$ of the within the Hessian partitioning, of the total charge density $\rho(\mathbf{r_b})$ evaluated at the *BCP*, corresponding to the *equilibrium geometry* and is used to construct *all* subsequent points along the $\mathbb{T}_\sigma(s)$. This real space frame of reference has been referred to as $\mathbb{U}_\sigma$-space [*J. Am. Chem. Soc.* **141**, 5497–5503 (2019)] [*Journal of Computational Chemistry* **410**(21), 1881-1891 (2019)] [*Chemical Physics Letters* **722**, 110–118, (2019)] [*Int J Quantum Chem* **118**(16) e25676 (2018).] [*Int J Quantum Chem* **118**(13), e25565 (2017)] [*Chem. Phys. Lett.* **667**, 25–31 (2017)] however, this nomenclature is unnecessarily complex and so we won't use it in the main text. The $\mathbb{T}_\sigma(s)$ is constructed using the change in position of the *BCP*, for all displacement steps **dr** of the *BCP* in the calculation. Each *BCP* shift vector **dr** is mapped to a point $\{(\underline{\mathbf{e}}_{1\sigma}\cdot\mathbf{dr}), (\underline{\mathbf{e}}_{2\sigma}\cdot\mathbf{dr}), (\underline{\mathbf{e}}_{3\sigma}\cdot\mathbf{dr})\}$ in sequence, forming the $\mathbb{T}_\sigma(s)$. This mapping is sufficiently symmetry breaking to distinguish stereo-isomers and isotopomers with degenerate relative energies. In contrast, *conventional* QTAIM is confined to the use of scalar measures and therefore can only magnify differences that may exist in relative energies associated with different structures. Conventional QTAIM cannot therefore distinguish stereo-isomers that have degenerate, i.e. equal, relative energies.

Numerical considerations for calculations of the trajectories:

Central to the concept of the trajectories $\mathbb{T}_\sigma(s)$ is the concept of a monotonically increasing sequence parameter *s*, which may take the form of an increasing integer sequence (0, 1, 2, 3,...) in applications where a set of discrete numbered steps are involved, or a continuous real number. The 3-D stress tensor trajectory $\mathbb{T}_\sigma(s)$ is then defined as an ordered set of points, whose sequence is described by the parameter *s*. In this application, we used an integer step number for *s*. We first choose to associate $s = 0$ with a specific reference molecular graph, in this case, the energy minimum structure. For a specific *BCP*, the coordinates associated with each of the points are calculated by evaluating the components of the shift vector $\mathbf{dr} = \mathbf{r_b}(s) - \mathbf{r_b}(s\text{-}1)$ where $\mathbf{r_b}$ indicates the location of the *BCP*, from the previous step to the current step in the reference coordinate frame defined by the eigenvectors $\underline{\mathbf{e}}_{1\sigma}$, $\underline{\mathbf{e}}_{2\sigma}$, $\underline{\mathbf{e}}_{3\sigma}$.

Note: for <u>displaying</u> the QTAIM $\mathbb{T}(s)$ and stress tensor trajectories $\mathbb{T}_\sigma(s)$, large steps that can occur at the beginning or end of a stress tensor trajectory $\mathbb{T}_\sigma(s)$ may swamp the appearance of the stress tensor trajectory $\mathbb{T}_\sigma(s)$. To solve this we temporarily filter these steps before including them back in to correctly calculate the $\mathbb{U}_\sigma$-space stress tensor trajectory $\mathbb{T}_\sigma(s)$.

The calculation of the $\mathbb{T}_\sigma(s)$ is made easier if the code which produces the list of structures corresponding to points along each step of the torsion (CW) ($-180.0^o \leq \theta \leq 0.0^o$) and counterclockwise CCW ($0.0^o \leq \theta \leq$

+180.0º) generates these structures at regularly-spaced points along. The consequence of this desirable characteristic is that there are few or no large changes or 'spikes' in the magnitude of the *BCP* shift vector **dr** i.e. Δ**dr**, between path step *s* and *s* + 1. Such anomalies occur because some path-following algorithms may employ occasional small predictor-corrector steps that are at least an order of magnitude smaller than standard steps. In this analysis it is observed that such intermittent relatively small steps in turn cause very small shifts **dr** to be interspersed between longer runs of larger changes, causing 'spike' noise in the otherwise smooth trajectories $\mathbb{T}(s)$. Such 'spikes', which usually only consist of a single spurious point deviating from the locally smooth stress tensor trajectory, can make potentially large spurious contributions to the stress tensor trajectory $\mathbb{T}_\sigma(s)$ and may be safely filtered. This filtering process was carried out manually in the current work.

In future to avoid the need to manually filter out these 'spikes', a combination of criteria are recommended for automated rejection of inclusion of a specific point into the trajectories $\mathbb{T}_\sigma(s)$:

1. If the magnitude of the **dr** associated with any current stress tensor trajectory point is less than 50% of the average of the corresponding **dr** values associated with the immediately preceding point and the immediately following point, the current point is filtered out as a 'spike'.
2. Abrupt changes in direction in the stress tensor trajectory $\mathbb{T}_\sigma(s)$, e.g. turning by more than 60^0 from one stress tensor trajectory $\mathbb{T}_\sigma(s)$ step to the next cause the current point to be labelled as a 'spike'.

These two rules taken together are referred to as the 'turn' filter. These rules can be repeatedly applied across multiple 'passes' through the stress tensor trajectory data as necessary.
It has been observed that the magnitudes of the steps **dr** naturally tend to slowly decrease toward the end of paths, corresponding to a slowed approach to an end minimum, and the corresponding part of the stress tensor trajectory $\mathbb{T}_\sigma(s)$ turns toward the $\mathbb{U}_\sigma$-space origin. A combination of the criteria mentioned above may be deployed to retain these parts of the stress tensor trajectory $\mathbb{T}_\sigma(s)$.

An alternative Kolmogorov-Zurbenko (W. Yang and I. Zurbenko, ***WIREs Comp Stat***, 2010, **2**, 340–351) data smoothing filter may also be applied.

1. Percentage deviation Δ**dr** of the magnitude of the **dr** from a moving average calculated along the stress tensor trajectory $\mathbb{T}_\sigma(s)$ exceeding a specific value should be 10% or less.
2. Abrupt changes in direction in the stress tensor trajectory $\mathbb{T}_\sigma(s)$, e.g. turning by more than $60^{\mathbf{o}}$ from one stress tensor trajectory $\mathbb{T}_\sigma(s)$ step to the next.

It has been observed that the magnitudes of the steps **dr** naturally tend to slowly decrease toward the end of paths, corresponding to a slowed approach to an end minimum, and the corresponding part of the stress tensor trajectory $\mathbb{T}_\sigma(s)$ turns toward the $\mathbb{U}_\sigma$-space origin. A combination of the criteria mentioned above may be

deployed to retain these parts of the stress tensor trajectory $\mathbb{T}_\sigma(s)$. A range of alternative traditional 'denoising' algorithms may also conceivably be usefully deployed.

I(iv). *Explanation of the stress tensor trajectory $\mathbb{T}_\sigma(s)$ in $\mathbb{U}_\sigma$-space:*

The calculation of the stress tensor trajectory $\mathbb{T}_\sigma(s)$ for the torsional *BCP* uses the frame of reference defined by the stress tensor eigenvectors $\{\pm\underline{\mathbf{e}}_{1\sigma},\pm\underline{\mathbf{e}}_{2\sigma},\pm\underline{\mathbf{e}}_{3\sigma}\}$ at the torsional *BCP*. This frame of reference is referred to as the stress tensor trajectory space ($\mathbb{U}_\sigma$-space) is also used to construct *all* subsequent points along the $\mathbb{T}_\sigma(s)$ for dihedral torsion angles in the range $-180.0^o \leq \theta \leq +180.0^o$, where $\theta = 0.0^o$ usually corresponds to the minimum energy geometry. We adopt the convention that CW circular rotations for the range $-180.0° \leq \theta \leq 0.0°$ and CCW circular rotations for the range $0.0° \leq \theta \leq +180.0°$. The change in position of the *BCP* in the $\mathbb{U}_\sigma$-space is used to construct the $\mathbb{T}_\sigma(s)$ using the displacement steps **dr** of the calculation. Each finite *BCP* displacement vector **dr** is mapped to a point $\{(\underline{\mathbf{e}}_{1\sigma}\cdot\mathbf{dr}), (\underline{\mathbf{e}}_{2\sigma}\cdot\mathbf{dr}), (\underline{\mathbf{e}}_{3\sigma}\cdot\mathbf{dr})\}$ in sequence, forming the $\mathbb{T}_\sigma(s)$, that is constructed from the vector dot products (the dot product is a projection: a measure of vectors being parallel to each other) of the stress tensor $\mathbb{T}_\sigma(s)$ eigenvector components evaluated at the *BCP.* The projections of the *BCP* displacements **dr** are associated with the bond torsion: $\underline{\mathbf{e}}_{1\sigma}.\mathbf{dr} \rightarrow$ bond-twist, $\underline{\mathbf{e}}_{2\sigma}.\mathbf{dr} \rightarrow$ bond-flexing and $\underline{\mathbf{e}}_{3\sigma}.\mathbf{dr} \rightarrow$ bond-axiality [*J. Am. Chem. Soc*. **141**, 5497–5503 (2019)] [*Int. J. Quantum Chem*. **118**, e25565 (2018)] [*Int. J. Quantum Chem*. **118**, e25676 (2018)] [*Chem. Phys. Lett*. **667**, 25–31 (2017)] [*J. Comput. Chem.* **40**, 1881–1891 (2019)] [*Chem. Phys. Lett.* **722**, 110–118 (2019)] [*Phys. Chem. Chem. Phys*. **22**, 2509–2520 (2020)].

The gap that we observe for the $\mathbb{T}_\sigma(s)$ between the CCW and CW torsions at a torsion $\theta = 0.0^o$ is due to their *BCP* shift vectors **dr** being oppositely directed and of non-zero magnitude. For example for a CCW torsion starting at $\theta = 0.0^o$ with a finite *BCP* shift **dr = {+0.01, 0.00, 0.00}**, the corresponding CW finite *BCP* shift **dr ≈ {-0.01, 0.00, 0.00},** giving a $\mathbb{U}_\sigma$-space separation of the $\mathbb{T}_\sigma(s)$ of the CCW and CW torsions at a torsion $\theta = 0.0^o$ of approximately 0.01-(-0.01) = 0.02. This mapping is sufficiently symmetry breaking to enable the $\mathbb{T}_\sigma(s)$ of S and R stereoisomers at the equilibrium configuration to be distinguished, in contrast to conventional *scalar* QTAIM. The $\mathbb{T}_\sigma(s)$ comprises a series of contiguous points as a 3-D vector path displaying the effect of the structural change and is analyzed here in terms of the CW and CCW directions of bond torsion. The $\underline{\mathbf{e}}_{1\sigma}$ corresponds to the *most* preferred direction of charge density $\rho(\mathbf{r})$ accumulation and therefore the most facile direction in the plane perpendicular to the bond-path, where bond-torsion about the *BCP* does not involve structural distortion in the form of any increase in bond-path length from the straight-line bonded separation. A value of $\{\underline{\mathbf{e}}_{1\sigma}.\mathbf{dr}\}_{\mathbf{max}} = 0.0$ corresponds to a constant orientation of the $\underline{\mathbf{e}}_{1\sigma}$ eigenvector in real space and therefore constant bond-path torsion (bond-twist). The subscript "$_{\mathbf{max}}$" corresponds to the difference between

the minimum and maximum value of the projection of the *BCP* shift **dr** onto $\underline{\mathbf{e}}_{1\sigma}$ or $\underline{\mathbf{e}}_{2\sigma}$ or $\underline{\mathbf{e}}_{3\sigma}$ along the entire stress tensor trajectory $\mathbb{T}_{\sigma}(s)$, see **Tables 1-5**. We will denote the maximum stress tensor projections $\mathbb{T}_{\sigma}(s)_{max}$ = **{**bond-twist$_{max}$, bond-flexing$_{max}$, bond-anharmonicity$_{max}$}; these quantities therefore define the dimensions of a 'bounding box' around each $\mathbb{T}_{\sigma}(s)$. The $\underline{\mathbf{e}}_{2\sigma}$ corresponds to the *least* preferred, i.e. the least readily distorted, direction of charge density $\rho(\mathbf{r})$ accumulation and therefore least facile direction in the plane perpendicular to the bond-path. This is because bond-flexing requires a greater structural distortion than bond-twist (torsion) in the form of an increase in bond-path length from the straight-line bonded separation. A value $\{\underline{\mathbf{e}}_{2\sigma}.\mathbf{dr}\}_{max} = 0.0$ corresponds to constant bond-flexing in real space. A value of $\{\underline{\mathbf{e}}_{3\sigma}.\mathbf{dr}\}_{max} > 0.0$ indicates the bond-axiality corresponding to a changing *BCP* shift **dr** in real space relative to the bond-path, and therefore greater freedom for the *BCP* to slide along the bond-path; note the bond-axiality axis label in **Figures 2**. Conversely, $\{\underline{\mathbf{e}}_{3\sigma}.\mathbf{dr}\}_{max} = 0.0$ corresponds to a constant *BCP* shift **dr** in real space along the bond-path and therefore an absence of bond-axiality.

2. Supplementary Materials S2. Distance measures for alanine with and without an applied electric field.

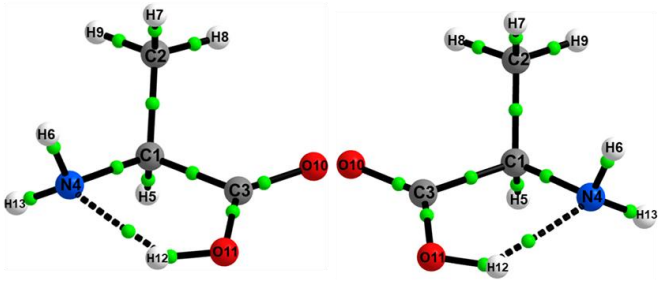
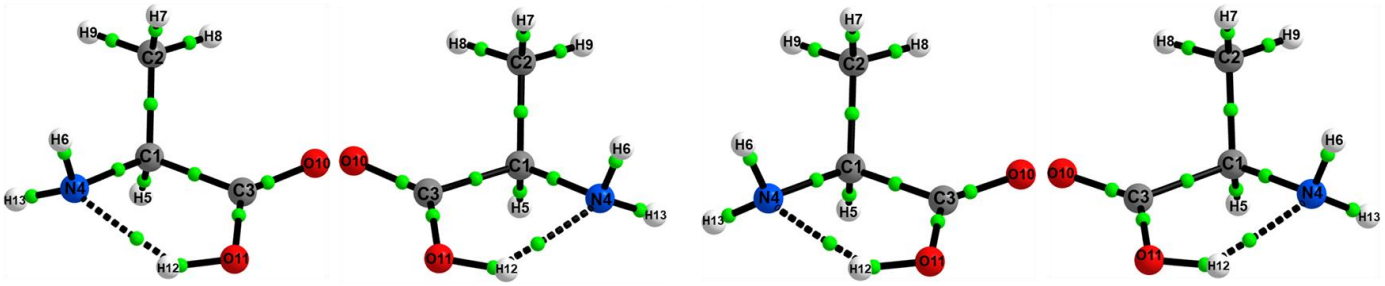
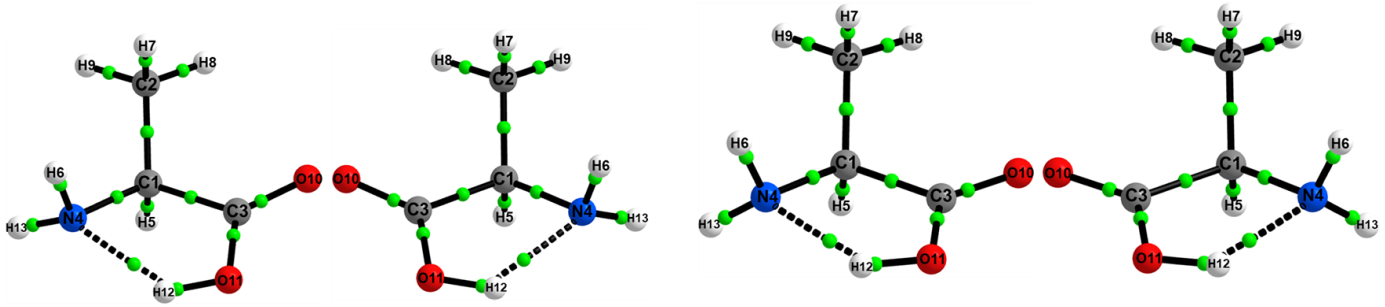


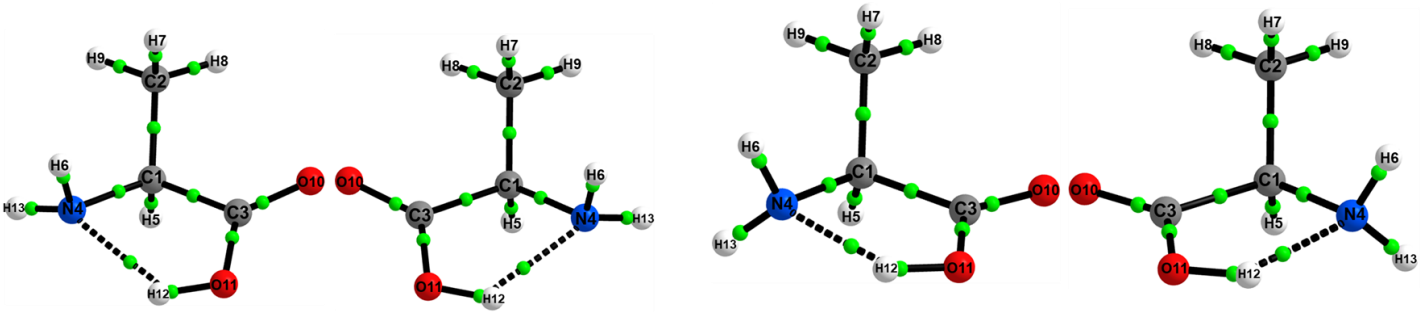
Figure S2(I). The S_a (left panels) and R_a (right panels) pairs of molecular graphs for **E**-field =0 a.u for values of the torsion θ = 0.0º. The unlabeled green spheres indicate the bond critical points (*BCP*s).



(a)



(b)



(c)

Figure S2(II). The S_a(left panels) and R_a(right panels) pairs of molecular graphs for **E**-field = $\pm 25\times10^{-4}$ a.u, (sub-figure **(a)**), **E** = $\pm 50\times10^{-4}$ a.u (sub-figure **(b)**) and **E** = $\pm 100\times10^{-4}$ a.u (sub-figure **(c)**) in the applied electric **(E)**-fields (in a.u.) for values of the torsion θ = 0.0º. The **E**-field values < 0 are provided in the left panel, the **E**-field values > 0 are provided in the right panel. The unlabeled green spheres indicate the bond critical points (*BCP*s).

2. Supplementary Materials S2. Distance measures for alanine with and without an applied electric field. (continued)

Table S2(a). The distance measures of the S_a and R_a stereoisomers of alanine without an applied electric field (in a.u.) for values of the torsion $\theta = 0.0^o$. Values of the inter-nuclear separations are referred to as the geometric bond-lengths (GBL) and bond-path lengths (BPL) (in a.u.).

	GBL	BPL	(C1-*BCP*,*BCP*-C2)	(C1-*BCP*,*BCP*-C3)	(C2-*BCP*,*BCP*-H9)
			S_a		
E-field = 0 a.u					
BCP					
C1-C2	2.8846	2.8849	(1.4783, 1.4066)	(---,---)	(---,---)
C1-C3	2.9175	2.9188	(---,---)	(1.4196, 1.4992)	(---,---)
C2-H9	2.0587	2.0411	(---,---)	(---,---)	(1.2688, 0.7723)
			R_a		
E-field = 0 a.u					
BCP					
C1-C2	2.8846	2.8849	(1.4783, 1.4066)	(---,---)	(---,---)
C1-C3	2.9175	2.9188	(---,---)	(1.4196, 1.4992)	(---,---)
C2-H9	2.0587	2.0411	(---,---)	(---,---)	(1.2688, 0.7723)

2. Supplementary Materials S2. Distance measures for alanine with and without an applied electric field. (continued)

Table S2(b). The distance measures of the S_a and R_a stereoisomers of alanine with an applied electric field (in a.u.) for values of the torsion θ = 0.0º. Values of the inter-nuclear separations are referred to as the geometric bond-lengths (GBL) and bond-path lengths (BPL) (in a.u.).

	GBL	BPL	(C1-*BCP*,*BCP*-C2)	(C1-*BCP*,*BCP*-C3)	(C2-*BCP*,*BCP*-H9)
			S_a		
E-field = -25×10^{-4} a.u					
BCP					
C1-C2	2.8826	2.8829	(1.4728, 1.4100)	(---,---)	(---,---)
C1-C3	2.9153	2.9167	(---,---)	(1.4273, 1.4894)	(---,---)
C2-H9	2.0608	2.0318	(---,---)	(---,---)	(1.2979, 0.7339)
E-field = -50×10^{-4} a.u					
BCP					
C1-C2	2.8810	2.8813	(1.4757, 1.4056)	(---,---)	(---,---)
C1-C3	2.9146	2.9159	(---,---)	(1.4186, 1.4973)	(---,---)
C2-H9	2.0615	2.0439	(---,---)	(---,---)	(1.2701, 0.7738)
E-field = -100×10^{-4} a.u					
BCP					
C1-C2	2.8777	2.8780	(1.4733, 1.4047)	(---,---)	(---,---)
C1-C3	2.9137	2.9150	(---,---)	(1.4181, 1.4969)	(---,---)
C2-H9	2.0631	2.0455	(---,---)	(---,---)	(1.2707, 0.7748)
			R_a		
E-field = -25×10^{-4} a.u					
BCP					
C1-C2	2.8826	2.8829	(1.4728, 1.4100)	(---,---)	(---,---)
C1-C3	2.9153	2.9167	(---,---)	(1.4273, 1.4894)	(---,---)
C2-H9	2.0608	2.0318	(---,---)	(---,---)	(1.2979, 0.7339)
E-field = -50×10^{-4} a.u					
BCP					
C1-C2	2.8810	2.8813	(1.4757, 1.4056)	(---,---)	(---,---)
C1-C3	2.9146	2.9159	(---,---)	(1.4186, 1.4973)	(---,---)
C2-H9	2.0615	2.0439	(---,---)	(---,---)	(1.2701, 0.7738)
E-field = -100×10^{-4} a.u					
BCP					
C1-C2	2.8777	2.8780	(1.4733, 1.4047)	(---,---)	(---,---)
C1-C3	2.9137	2.9150	(---,---)	(1.4181, 1.4969)	(---,---)
C2-H9	2.0631	2.0455	(---,---)	(---,---)	(1.2707, 0.7748)

2. Supplementary Materials S2. Distance measures for alanine with and without an applied electric field. (continued)

Table S2(b). The distance measures of the S_a and R_a stereoisomers of alanine with an applied electric field (in a.u.) for values of the torsion θ = 0.0º. Values of the inter-nuclear separations are referred to as the geometric bond-lengths (GBL) and bond-path lengths (BPL) (in a.u.).

	GBL	BPL	(C1-*BCP*,*BCP*-C2)	(C1-*BCP*,*BCP*-C3)	(C2-*BCP*,*BCP*-H9)
			S_a		
E-field = +25 a.u					
BCP					
C1-C2	2.8857	2.8860	(1.4752, 1.4108)	(---,---)	(---,---)
C1-C3	2.9172	2.9185	(---,---)	(1.4281, 1.4904)	(---,---)
C2-H9	2.0597	2.0307	(---,---)	(---,---)	(1.2976, 0.7331)
E-field = +50×10^{-4} a.u					
BCP					
C1-C2	2.8871	2.8874	(1.4806, 1.4068)	(---,---)	(---,---)
C1-C3	2.9184	2.9196	(---,---)	(1.4202, 1.4993)	(---,---)
C2-H9	2.0592	2.0416	(---,---)	(---,---)	(1.2696, 0.7720)
E-field = +100×10^{-4} a.u					
BCP					
C1-C2	2.8896	2.8899	(1.4828, 1.4071)	(---,---)	(---,---)
C1-C3	2.9206	2.9217	(---,---)	(1.4213, 1.5005)	(---,---)
C2-H9	2.0586	2.0409	(---,---)	(---,---)	(1.2697, 0.7713)
			R_a		
E-field = +25×10^{-4} a.u					
BCP					
C1-C2	2.8857	2.8860	(1.4752, 1.4108)	(---,---)	(---,---)
C1-C3	2.9172	2.9185	(---,---)	(1.4281, 1.4904)	(---,---)
C2-H9	2.0597	2.0307	(---,---)	(---,---)	(1.2976, 0.7331)
E-field = +50×10^{-4} a.u					
BCP					
C1-C2	2.8871	2.8874	(1.4806, 1.4068)	(---,---)	(---,---)
C1-C3	2.9184	2.9196	(---,---)	(1.4202, 1.4993)	(---,---)
C2-H9	2.0592	2.0416	(---,---)	(---,---)	(1.2696, 0.7720)
E-field = +100×10^{-4} a.u					
BCP					
C1-C2	2.8896	2.8899	(1.4828, 1.4071)	(---,---)	(---,---)
C1-C3	2.9206	2.9217	(---,---)	(1.4213, 1.5005)	(---,---)
C2-H9	2.0586	2.0409	(---,---)	(---,---)	(1.2697, 0.7713)

2. Supplementary Materials S2. Distance measures for alanine with and without an applied electric field. (continued)

Table S2(c). The relative distance measures of the the S_a and R_a stereoisomers of alanine for the applied electric **(E)**-fields (in a.u.) for values of the torsion θ = 0.0º are provided. Values of the inter-nuclear separations are referred to as the geometric bond-lengths (ΔGBL) and bond-path lengths (ΔBPL) (in a.u.).

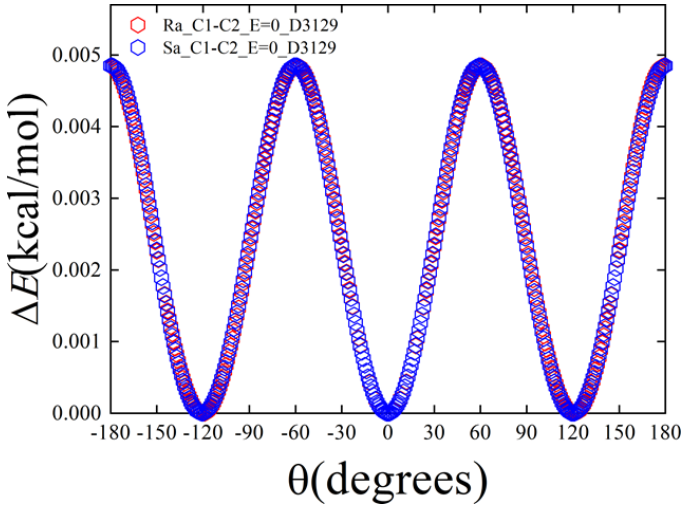
	ΔGBL	ΔBPL	Δ(C1-*BCP*,*BCP*-C2)	Δ(C1-*BCP*,*BCP*-C3)	Δ(C2-*BCP*,*BCP*-H9)
			S_a		
E-field = -25×10^{-4} a.u					
BCP					
C1-C2	-0.0020	-0.0020	(-0.0055, 0.0034)	(---,---)	(---,---)
C1-C3	-0.0022	-0.0021	(---,---)	(0.0077, -0.0098)	(---,---)
C2-H9	0.0021	-0.0093	(---,---)	(---,---)	(0.0291, -0.0384)
E-field = -50×10^{-4} a.u					
BCP					
C1-C2	-0.0036	-0.0036	(-0.0026, -0.0010)	(---,---)	(---,---)
C1-C3	-0.0029	-0.0029	(---,---)	(-0.0010, -0.0019)	(---,---)
C2-H9	0.0028	0.0028	(---,---)	(---,---)	(0.0013, 0.0015)
E-field = -100×10^{-4} a.u					
BCP					
C1-C2	-0.0069	-0.0069	(-0.0050, -0.0019)	(---,---)	(---,---)
C1-C3	-0.0038	-0.0038	(---,---)	(-0.0015, -0.0023)	(---,---)
C2-H9	0.0044	0.0044	(---,---)	(---,---)	(0.0019, 0.0025)
			R_a		
E-field = -25×10^{-4} a.u					
BCP					
C1-C2	-0.0020	-0.0020	(-0.0055, 0.0034)	(---,---)	(---,---)
C1-C3	-0.0022	-0.0021	(---,---)	(0.0077, -0.0098)	(---,---)
C2-H9	0.0021	-0.0093	(---,---)	(---,---)	(0.0291, -0.0384)
E-field = -50×10^{-4} a.u					
BCP					
C1-C2	-0.0036	-0.0036	(-0.0026, -0.0010)	(---,---)	(---,---)
C1-C3	-0.0029	-0.0029	(---,---)	(-0.0010, -0.0019)	(---,---)
C2-H9	0.0028	0.0028	(---,---)	(---,---)	(0.0013, 0.0015)
E-field = -100×10^{-4} a.u					
BCP					
C1-C2	-0.0069	-0.0069	(-0.0050, -0.0019)	(---,---)	(---,---)
C1-C3	-0.0038	-0.0038	(---,---)	(-0.0015, -0.0023)	(---,---)
C2-H9	0.0044	0.0044	(---,---)	(---,---)	(0.0019, 0.0025)

2. Supplementary Materials S2. Distance measures for alanine with and without an applied electric field. (continued)

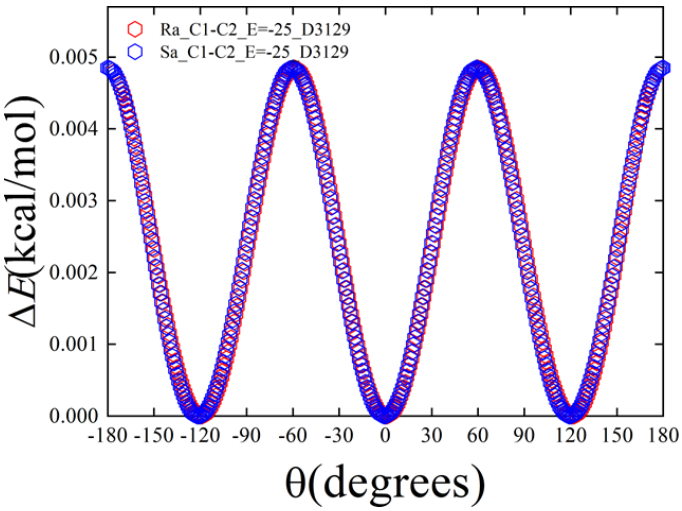
Table S2(c). The relative distance measures of the the S_a and R_a stereoisomers of alanine for the applied electric **(E)**-fields (in a.u.) for values of the torsion $\theta = 0.0^o$ are provided. Values of the inter-nuclear separations are referred to as the geometric bond-lengths (ΔGBL) and bond-path lengths (ΔBPL) (in a.u.).

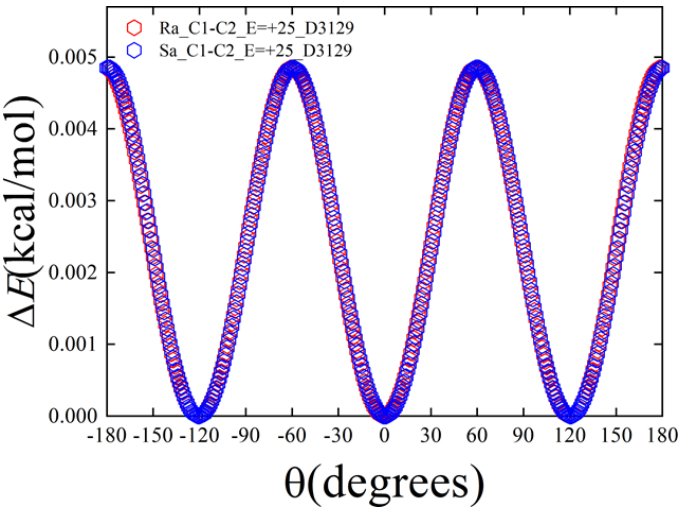
	ΔGBL	ΔBPL	Δ(C1-*BCP*,*BCP*-C2)	Δ(C1-*BCP*,*BCP*-C3)	Δ(C2-*BCP*,*BCP*-H9)
			S_a		
E-field = +25×10^{-4} a.u					
BCP					
C1-C2	0.0011	0.0011	(-0.0031, 0.0042)	(---,---)	(---,---)
C1-C3	-0.0003	-0.0003	(---,---)	(0.0085, -0.0088)	(---,---)
C2-H9	0.0010	-0.0104	(---,---)	(---,---)	(0.0288, -0.0392)
E-field = +50×10^{-4} a.u					
BCP					
C1-C2	0.0025	0.0025	(0.0023, 0.0002)	(---,---)	(---,---)
C1-C3	0.0009	0.0008	(---,---)	(0.0006, 0.0001)	(---,---)
C2-H9	0.0005	0.0005	(---,---)	(---,---)	(0.0008, -0.0003)
E-field = +100×10^{-4} a.u					
BCP					
C1-C2	0.0050	0.0050	(0.0045, 0.0005)	(---,---)	(---,---)
C1-C3	0.0031	0.0029	(---,---)	(0.0017, 0.0013)	(---,---)
C2-H9	-0.0001	-0.0002	(---,---)	(---,---)	(0.0009, -0.0010)
			R_a		
E-field = +25×10^{-4} a.u					
BCP					
C1-C2	0.0011	0.0011	(-0.0031, 0.0042)	(---,---)	(---,---)
C1-C3	-0.0003	-0.0003	(---,---)	(0.0085, -0.0088)	(---,---)
C2-H9	0.0010	-0.0104	(---,---)	(---,---)	(0.0288, -0.0392)
E-field = +50×10^{-4} a.u					
BCP					
C1-C2	0.0025	0.0025	(0.0023, 0.0002)	(---,---)	(---,---)
C1-C3	0.0009	0.0008	(---,---)	(0.0006, 0.0001)	(---,---)
C2-H9	0.0005	0.0005	(---,---)	(---,---)	(0.0008, -0.0003)
E-field = +100×10^{-4} a.u					
BCP					
C1-C2	0.0050	0.0050	(0.0045, 0.0005)	(---,---)	(---,---)
C1-C3	0.0031	0.0029	(---,---)	(0.0017, 0.0013)	(---,---)
C2-H9	-0.0001	-0.0002	(---,---)	(---,---)	(0.0009, -0.0010)

2. Supplementary Materials S2. Distance measures for alanine with and without an applied electric field. (continued)

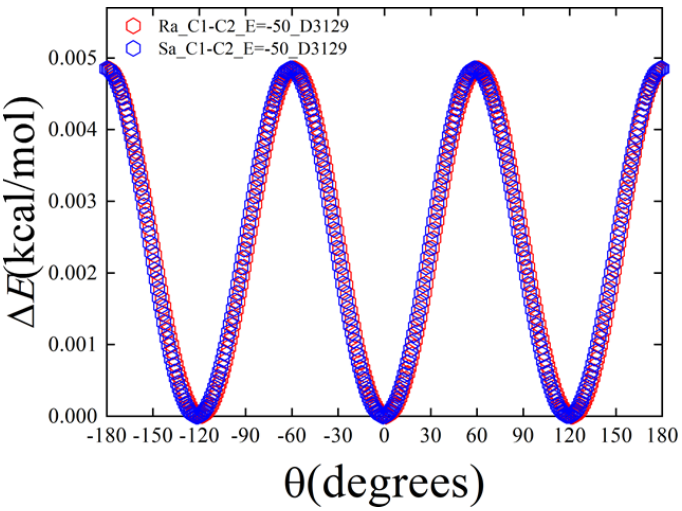


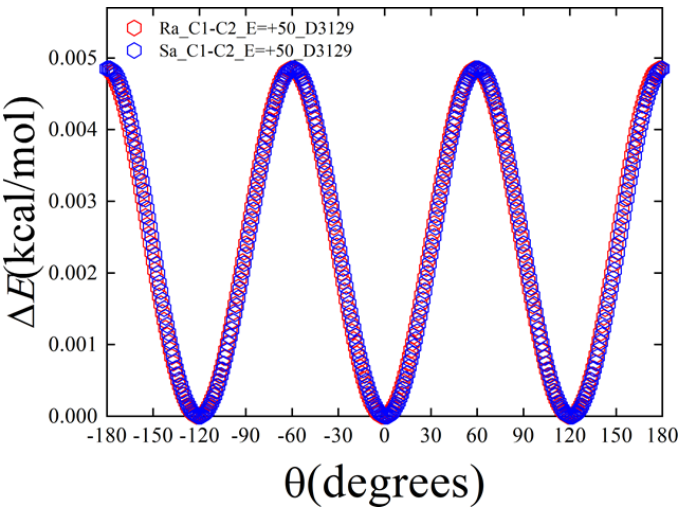
(a)





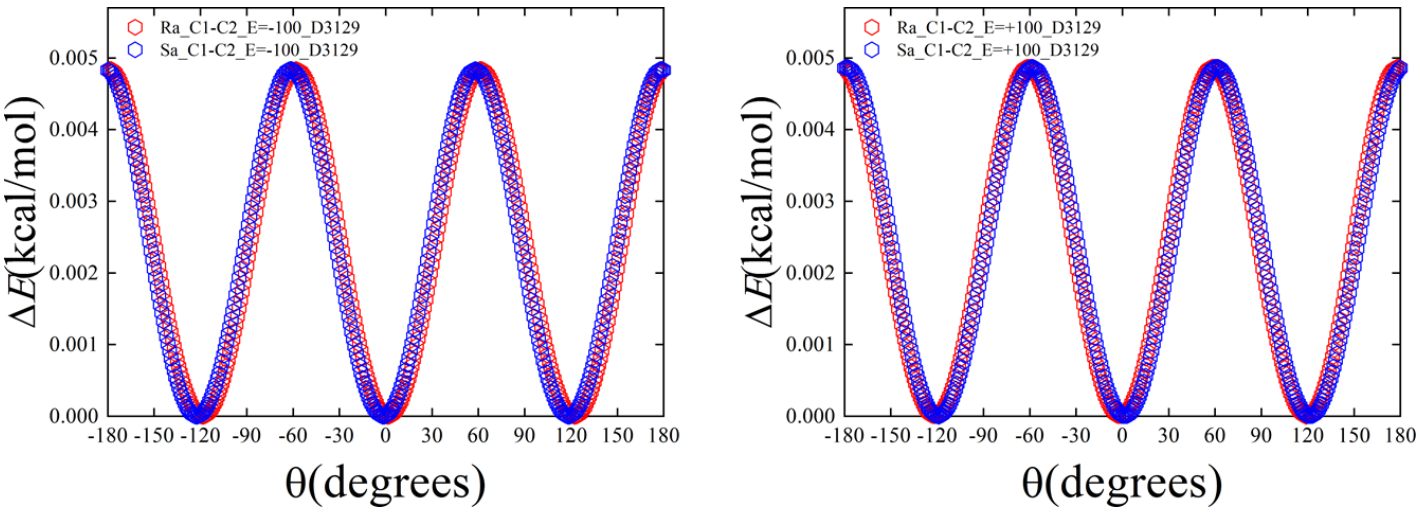
(b)





(c)

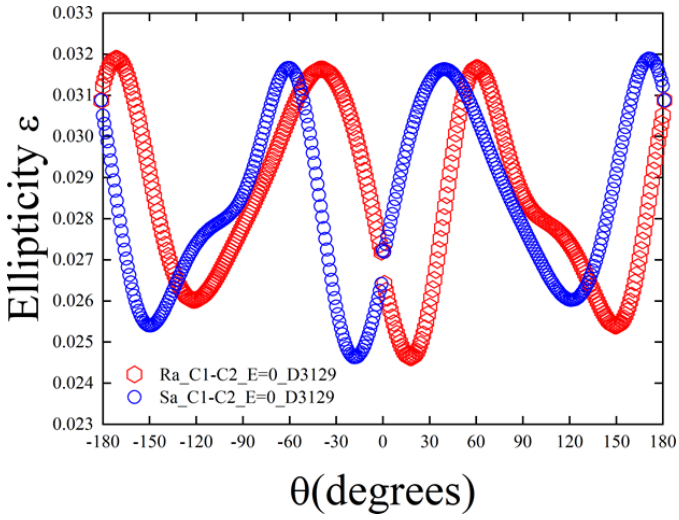
2. Supplementary Materials S2. Distance measures for alanine with and without an applied electric field. (continued)



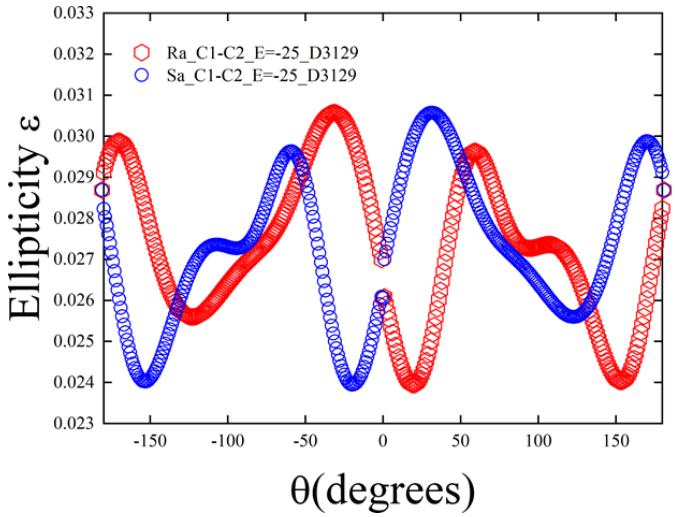
(d)

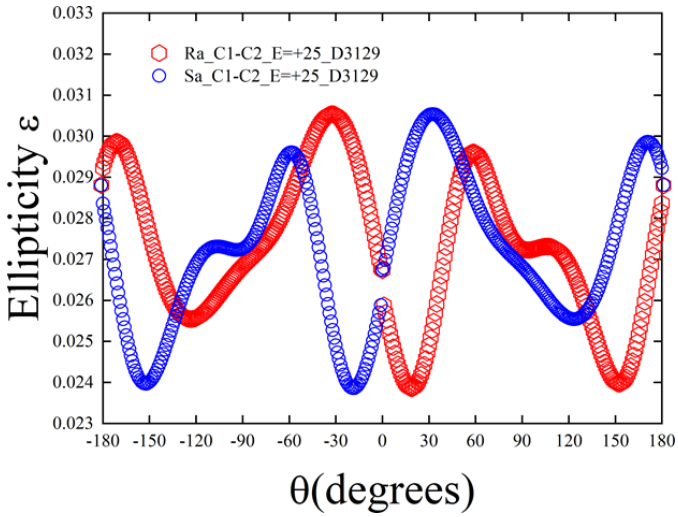
Figure S2(III). The variation of the relative energy ΔE of the torsional θ C1-C2 *BCP* with the CW and CCW for the S_a and R_a stereoisomers for **E**-field = 0 a.u, (sub-figure **(a)**) **E**-field = $\pm 25\times10^{-4}$ a.u, (sub-figure **(b)**), **E** = $\pm 50 \times10^{-4}$ a.u (sub-figure **(c)**) and **E** = $\pm 100\times10^{-4}$ a.u (sub-figure **(d)**) in the applied electric **(E)**-fields (in a.u.). The **E**-field values < 0 are provided in the left panel, the **E**-field values > 0 are provided in the right panel.

3. Supplementary Materials S3. Scalar measures with for alanine with and without an applied electric field.

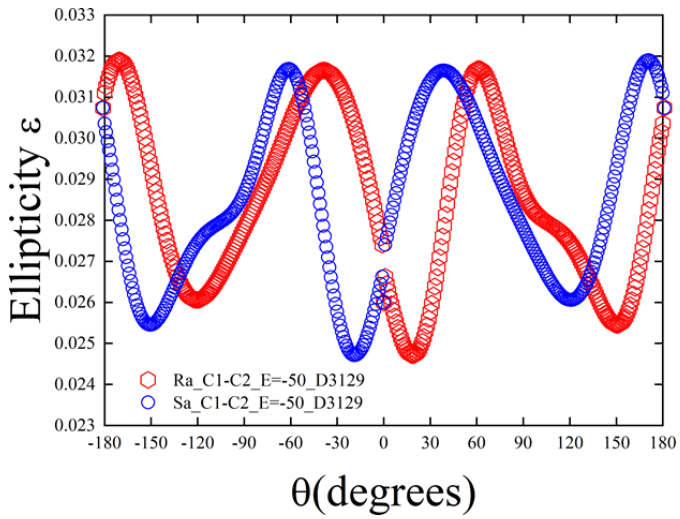


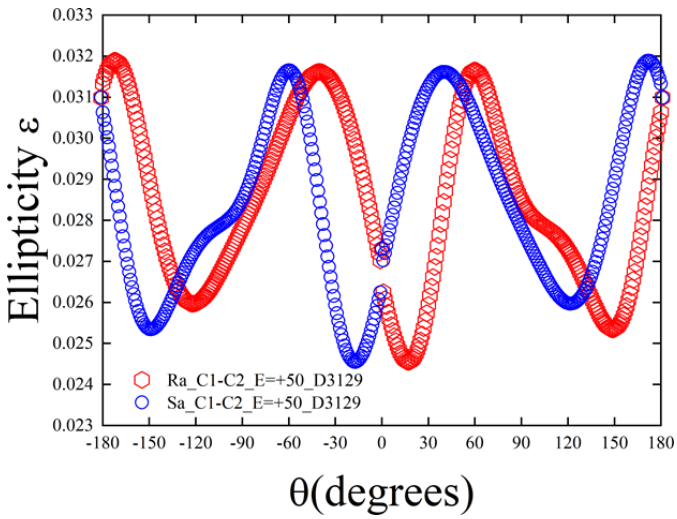
(a)





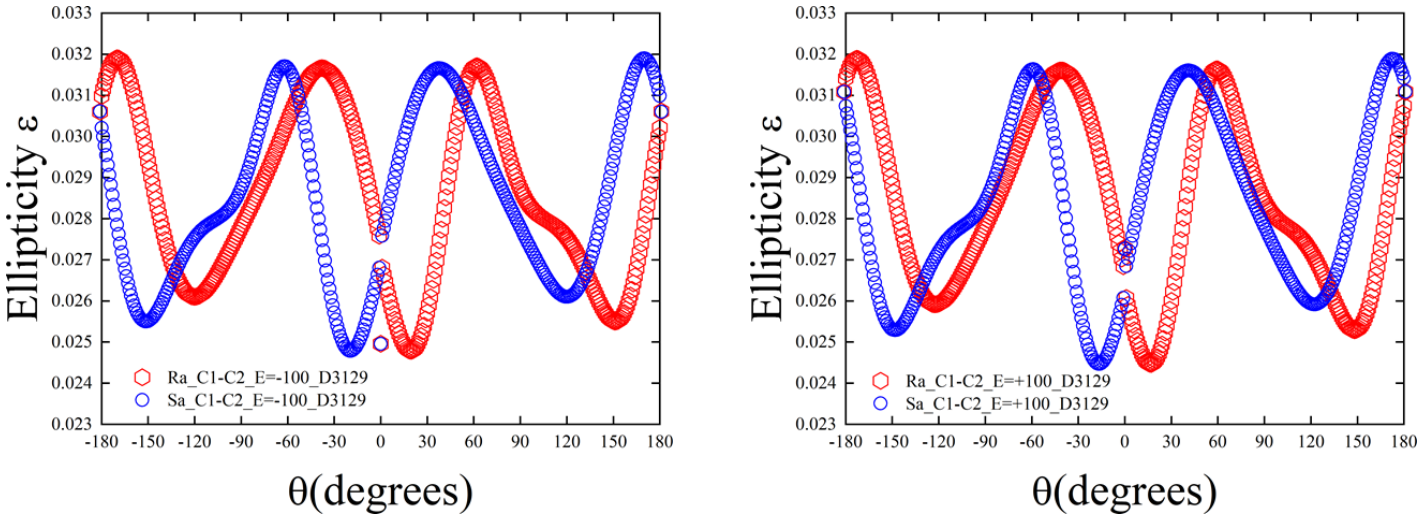
(b)





(c)

3. Supplementary Materials S3. Scalar measures with for alanine with and without an applied electric field. (continued)



(d)

Figure S3(I). The variation of the ellipticity ε with θ for the torsion of C1-C2 *BCP* with the CW and CCW for the S_a and R_a stereoisomers for **E**-field = 0 a.u, (sub-figure **(a)**) **E**-field = $\pm 25\times10^{-4}$ a.u, (sub-figure **(b)**), **E** = $\pm 50 \times10^{-4}$ a.u (sub-figure **(c)**) and **E** = $\pm 100\times10^{-4}$ a.u (sub-figure **(d)**) in the applied electric **(E)**-fields (in a.u.). The **E**-field values < 0 are provided in the left panel, the **E**-field values > 0 are provided in the right panel.

4. Supplementary Materials S4. Additional $\mathbb{T}_\sigma(s)$ and tables of the alanine torsional C1-C2 *BCPs*.

Table S4(a). The maximum stress tensor projections **{**bond-twist $_{max}$, bond-flexing $_{max}$, bond-axiality$_{max}$} for the dominant torsional C1-C2 *BCP* of alanine subjected to an electric field are presented; all entries have been multiplied by 10^3.

{bond-twist$_{max}$, bond-flexing$_{max}$, bond-axiality$_{max}$}

	S_a		R_a	
	CW	**CCW**	**CW**	**CCW**
C1-C2 *BCP*				
E-field =0 a.u				
D3127	{0.6556, 2.3194, 0.8907}	{1.4191, 1.5024, 0.8492}	{1.4203, 1.5024, 0.8492}	{0.6568, 2.3194, 0.8906}
D3128	{0.8060, 2.0810, 0.8903}	{0.9693, 1.7184, 0.8429}	{0.9693, 1.7186, 0.8429}	{0.8059, 2.0811, 0.8882}
D3129	{0.5524, 2.0338, 0.8893}	{1.4425, 1.5643, 0.8526}	{1.4425, 1.5643, 0.8526}	{0.5524, 2.0338, 0.8893}
D4127	{1.1338, 2.4641, 0.8995}	{1.6212, 2.1859, 0.8665}	{1.6212, 2.1858, 0.8664}	{1.1338, 2.4641, 0.8995}
D4128	{0.9248, 2.7882, 0.8950}	{1.6870, 1.9044, 0.8641}	{1.6873, 1.9040, 0.8641}	{0.9248, 2.7884, 0.8950}
D4129	{1.2886, 2.5276, 0.8884}	{1.3137, 2.2575, 0.8763}	{1.3139, 2.2575, 0.8763}	{1.2888, 2.5275, 0.8884}
D5127	{1.1089, 2.1614,0.8934}	{1.3127, 2.0045, 0.8624}	{1.3127, 2.0043, 0.8624}	{1.1087, 2.1611, 0.8935}
D5128	{1.1075, 2.3156, 0.8906}	{1.0125, 1.6827, 0.8590}	{1.0125, 1.6827, 0.8590}	{1.1076, 2.3155, 0.8906}
D5129	{0.5426, 2.0994, 0.8851}	{1.4648, 1.9453, 0.8680}	{1.4648, 1.9453, 0.8680}	{0.5426, 2.0995, 0.8851}
E-field = -25×10^{-4} a.u				
D3127	{2.2535, 1.6740, 0.8511}	{2.3675, 1.1764, 0.7867}	{2.3675, 1.1764, 0.7867}	{2.2546, 1.6740, 0.8511}
D3128	{2.1559, 1.3472, 0.8543}	{2.3594, 1.4102, 0.7799}	{2.3594, 1.4102, 0.7799}	{2.1561, 1.3470, 0.8546}
D3129	{1.8953, 1.6273, 0.8495}	{2.4999, 1.1390, 0.7890}	{2.4999, 1.1390,0.7889}	{1.8953, 1.6272, 0.8496}
D4127	{2.2993, 1.7907, 0.8594}	{2.9574, 1.2619, 0.8125}	{2.9573, 1.2619, 0.8123}	{2.2993, 1.7907, 0.8596}
D4128	{2.3108, 1.8682, 0.8600}	{2.7144, 1.2791, 0.8113}	{2.7144, 1.2812, 0.8114}	{2.3107, 1.8683, 0.8599}
D4129	{2.4497, 1.5733, 0.8511}	{2.5899, 1.4252, 0.8226}	{2.5899, 1.4252, 0.8227}	{2.4498, 1.5732, 0.8510}
D5127	{2.0336, 1.6815, 0.8549}	{2.2809, 1.6555, 0.8001}	{2.2808, 1.6556, 0.8001}	{2.0337, 1.6815, 0.8552}
D5128	{1.8926, 1.8082, 0.8553}	{2.0900, 1.3256, 0.7959}	{2.0899, 1.3257, 0.7959}	{1.8926, 1.8080, 0.8554}
D5129	{1.7494, 1.5733, 0.8476}	{2.1460, 1.6501, 0.8043}	{2.1459, 1.6501, 0.8043}	{1.7494, 1.5732, 0.8475}
E-field = -50×10^{-4} a.u				
D3127	{1.2033, 2.5396, 0.9214}	{1.5666, 2.0525, 0.8554}	{1.5668, 2.0524, 0.8554}	{1.2033, 2.5396, 0.9216}
D3128	{1.2766, 2.1749, 0.9259}	{1.2731, 2.3948, 0.8496}	{1.2730, 2.3948, 0.8496}	{1.2766, 2.1748, 0.9259}
D3129	{0.8865, 2.3385, 0.9181}	{1.6651, 2.1707, 0.8601}	{1.6650, 2.1708, 0.8601}	{0.8864, 2.3385, 0.9181}
D4127	{1.3023, 2.5612, 0.9276}	{1.8870, 2.5657, 0.8778}	{1.8868, 2.5659, 0.8776}	{1.3023, 2.5611, 0.9277}
D4128	{1.0520, 2.7841, 0.9291}	{1.9473, 2.3698, 0.8802}	{1.9473, 2.3697, 0.8802}	{1.0520, 2.7841, 0.9292}
D4129	{1.3473, 2.5898, 0.9178}	{1.5839, 2.4812, 0.8914}	{1.5839, 2.4811, 0.8914}	{1.3472, 2.5899, 0.9175}
D5127	{1.5348, 2.2073, 0.9245}	{1.4968, 2.3214, 0.8673}	{1.4968, 2.3213, 0.8673}	{1.5348, 2.2073, 0.9245}
D5128	{1.4765, 2.2625, 0.9265}	{1.2859, 2.1493, 0.8655}	{1.2859, 2.1494, 0.8656}	{1.4765, 2.2625, 0.9263}
D5129	{1.0246, 2.1667, 0.9158}	{1.6280, 2.2059, 0.8739}	{1.6281, 2.2060, 0.8738}	{1.0246, 2.1667, 0.9158}
E-field = -100×10^{-4} a.u				
D3127	{1.1857, 2.4683, 0.9403}	{1.5317, 1.9655, 0.8749}	{1.5316, 1.9655, 0.8749}	{1.1858, 2.4684, 0.9403}
D3128	{1.2468, 2.1547, 0.9448}	{1.2491, 2.3001, 0.8703}	{1.2491, 2.3001, 0.8703}	{1.2467, 2.1546, 0.9448}
D3129	{0.8828, 2.3097, 0.9361}	{1.6412, 2.0781, 0.8827}	{1.6410, 2.0779, 0.8829}	{0.8828, 2.3097, 0.9360}
D4127	{1.3362, 2.5354, 0.9456}	{1.8788, 2.5007, 0.8946}	{1.8787, 2.5007, 0.8947}	{1.3361, 2.5353, 0.9456}
D4128	{1.0886, 2.7521, 0.9480}	{1.9590, 2.2988, 0.8994}	{1.9590, 2.2988, 0.8995}	{1.0885, 2.7521, 0.9478}
D4129	{1.4070, 2.5672, 0.9335}	{1.5717, 2.4415, 0.9113}	{1.5717, 2.4416, 0.9113}	{1.4069, 2.5672, 0.9335}
D5127	{1.4972, 2.2190, 0.9434}	{1.4508, 2.2874, 0.8870}	{1.4507, 2.2873, 0.8869}	{1.4972, 2.2190, 0.9434}
D5128	{1.4312, 2.2578, 0.9453}	{1.2496, 2.0928, 0.8871}	{1.2496, 2.0929, 0.8871}	{1.4312, 2.2577, 0.9453}
D5129	{1.0010, 2.1477, 0.9333}	{1.5913, 2.1842, 0.8964}	{1.5913, 2.1841, 0.8964}	{1.0010, 2.1477, 0.9332}

4. Supplementary Materials S4. Additional $\mathbb{T}_\sigma(s)$ and tables of the alanine torsional C1-C2 *BCPs.* (continued)

Table S4(a). The maximum stress tensor projections **{**bond-twist $_{max}$, bond-flexing $_{max}$, bond-axiality$_{max}$} for the dominant torsional C1-C2 *BCP* of alanine subjected to an electric field are presented; all entries have been multiplied by 10^3.

{bond-twist$_{max}$, bond-flexing$_{max}$, bond-axiality$_{max}$}

	S_a		R_a	
	CW	**CCW**	**CW**	**CCW**
C1-C2 *BCP*				
E-field = +25×10^{-4} a.u				
D3127	{2.1605, 1.9216, 0.8203}	{2.3480, 1.3947, 0.7569}	{2.3480, 1.3947, 0.7569}	{2.1603, 1.9215, 0.8204}
D3128	{2.1010, 1.5422, 0.8223}	{2.2974, 1.6772, 0.7516}	{2.2974, 1.6772, 0.7516}	{2.1011, 1.5423, 0.8224}
D3129	{1.7919, 1.8315, 0.8204}	{2.5131, 1.3838, 0.7571}	{2.5132, 1.3837, 0.7570}	{1.7920, 1.8315, 0.8204}
D4127	{2.1356, 1.9902, 0.8306}	{2.8429, 1.5258, 0.7889}	{2.8427, 1.5262, 0.7889}	{2.1342, 1.9884, 0.8300}
D4128	{2.1075, 2.1072, 0.8306}	{2.6537, 1.4992, 0.7839}	{2.6535, 1.4991, 0.7840}	{2.1076, 2.1071, 0.8306}
D4129	{2.2614, 1.8151, 0.8261}	{2.4947, 1.6505, 0.7948}	{2.4946, 1.6506, 0.7948}	{2.2613, 1.8151, 0.8261}
D5127	{2.0236, 1.8178, 0.8245}	{2.2300, 1.7500, 0.7710}	{2.2300, 1.7500, 0.7710}	{2.0236, 1.8179, 0.8244}
D5128	{1.8842, 1.9082, 0.8241}	{2.0021, 1.4855, 0.7658}	{2.0019, 1.4855, 0.7659}	{1.8842, 1.9083, 0.8241}
D5129	{1.6649, 1.7046, 0.8192}	{2.1289, 1.7371, 0.7724}	{2.1290, 1.7370, 0.7724}	{1.6649, 1.7046, 0.8192}
E-field = +50×10^{-4} a.u				
D3127	{1.3830, 2.5990, 0.8623}	{1.7672, 2.0716, 0.7940}	{1.7673, 2.0716, 0.7939}	{1.3829, 2.5989, 0.8622}
D3128	{1.4581, 2.1575, 0.8643}	{1.4934, 2.4770, 0.7907}	{1.4934, 2.4770, 0.7908}	{1.4580, 2.1577, 0.8645}
D3129	{1.0333, 2.3712, 0.8622}	{1.9035, 2.2063, 0.7939}	{1.9033, 2.2061, 0.7940}	{1.0331, 2.3711, 0.8623}
D4127	{1.3528, 2.5576, 0.8699}	{2.0481, 2.5027, 0.8277}	{2.0485, 2.5027, 0.8275}	{1.3529, 2.5577, 0.8699}
D4128	{1.1266, 2.7698, 0.8712}	{2.0711, 2.3262, 0.8219}	{2.0712, 2.3262, 0.8220}	{1.1266, 2.7698, 0.8711}
D4129	{1.3764, 2.5515, 0.8675}	{1.7517, 2.4314, 0.8322}	{1.7518, 2.4313, 0.8323}	{1.3764, 2.5514, 0.8678}
D5127	{1.6817, 2.1896, 0.8653}	{1.6849, 2.2508, 0.8071}	{1.6848, 2.2507, 0.8072}	{1.6821, 2.1898, 0.8655}
D5128	{1.6251, 2.2263, 0.8655}	{1.4718, 2.1147, 0.8030}	{1.4718, 2.1147, 0.8031}	{1.6251, 2.2263, 0.8655}
D5129	{1.1684, 2.1223, 0.8607}	{1.8248, 2.1609, 0.8079}	{1.8248, 2.1610, 0.8080}	{1.1686, 2.1223, 0.8607}
E-field = +100×10^{-4} a.u				
D3127	{1.5032,2.5241, 0.8241}	{1.9462, 2.0492, 0.7463}	{1.9462, 2.0492, 0.7462}	{1.5032,2.5242, 0.8242}
D3128	{1.5701, 2.0772, 0.8233}	{1.66432.44, 60, 0.7483}	{1.6645, 2.4462, 0.7483}	{1.5702, 2.0771, 0.8235}
D3129	{1.1415, 2.2724, 0.8230}	{2.0781, 2.1856, 0.7444}	{2.0780, 2.1856, 0.7445}	{1.1414, 2.2724, 0.8230}
D4127	{1.4386, 2.5202, 0.8266}	{2.1853, 2.4068, 0.7888}	{2.1851, 2.4066, 0.7888}	{1.4385, 2.5203, 0.8267}
D4128	{1.2461, 2.7011, 0.8295}	{2.1813, 2.2455, 0.7754}	{2.1812, 2.2454, 0.7753}	{1.2460, 2.7011, 0.8294}
D4129	{1.4467, 2.4553,0.8299}	{1.8801, 2.3656, 0.7860}	{1.8801, 2.3657, 0.7861}	{1.4468, 2.4552, 0.8298}
D5127	{1.7524, 2.1595, 0.8232}	{1.8480, 2.1928, 0.7590}	{1.8482, 2.1926, 0.7590}	{1.7528, 2.1596, 0.8233}
D5128	{1.6908, 2.1746, 0.8224}	{1.6019, 2.0552, 0.7538}	{1.6019, 2.0550, 0.7537}	{1.6907, 2.1746, 0.8223}
D5129	{1.2484, 2.0771, 0.8202}	{1.9637, 2.1080, 0.7564}	{1.9637, 2.1080, 0.7564}	{1.2482, 2.0770, 0.8204}

4. Supplementary Materials S4. Additional $\mathbb{T}_\sigma(s)$ and tables of the alanine torsional C1-C2 *BCPs.* (continued)

Table S4(b). The values of the chirality $\mathbb{C}_\sigma$ = $[(\mathbf{e_{1\sigma}\cdot dr})_{\mathbf{max}}]_{\mathbf{CCW}}$ - $[(\mathbf{e_{1\sigma}\cdot dr})_{\mathbf{max}}]_{\mathbf{CW}}$, bond-flexing $\mathbb{F}_\sigma$ = $[(\mathbf{e_{2\sigma}\cdot dr})_{\mathbf{max}}]_{\mathbf{CCW}}$ - $[(\mathbf{e_{2\sigma}\cdot dr})_{\mathbf{max}}]_{\mathbf{CW}}$, bond-axiality $\mathbb{A}_\sigma$ = $[(\mathbf{e_{3\sigma}\cdot dr})_{\mathbf{max}}]_{\mathbf{CCW}}$ - $[(\mathbf{e_{3\sigma}\cdot dr})_{\mathbf{max}}]_{\mathbf{CW}}$ and the chirality-helicity function $\mathbb{C}_{helicity} = \mathbb{C}_\sigma|\mathbb{A}_\sigma|$ of the torsional C1-C2 *BCP* of alanine are presented, all entries are multiplied by 10^3.

C1-C2 *BCP*	S_a $\{\mathbb{C}_\sigma, \mathbb{F}_\sigma, \mathbb{A}_\sigma\}$	$\mathbb{C}_{helicity}$ $[\mathbb{C}_\sigma,\|\mathbb{A}_\sigma\|]$	R_a $\{\mathbb{C}_\sigma, \mathbb{F}_\sigma, \mathbb{A}_\sigma\}$
E-field =0 a.u			
D3127	{0.7635**[S_σ]**, -0.8171**[R_σ]**, -0.0415**[R_σ]**}	1.1604**[S_σ, S_σ]**	{-0.7635**[R_σ]**,0.8170**[S_σ]**, 0.0414**[S_σ]**}
D3128	{0.1633**[S_σ]**, -0.3626**[R_σ]**, -0.0474**[R_σ]**}		{-0.1634**[R_σ]**, 0.3625**[S_σ]**, 0.0453**[S_σ]**}
D3129	{0.8901**[S_σ]**, -0.4695**[R_σ]**, -0.0367**[R_σ]**}		{-0.8901**[R_σ]**, 0.4694**[S_σ]**, 0.0367**[S_σ]**}
D4127	{0.4874**[S_σ]**, -0.2782**[R_σ]**, -0.0330**[R_σ]**}		{-0.4874**[R_σ]**, 0.2783**[S_σ]**, 0.0331**[S_σ]**}
D4128	{0.7623**[S_σ]**, -0.8838**[R_σ]**, -0.0309**[R_σ]**}		{-0.7624**[R_σ]**, 0.8844**[S_σ]**, 0.0309**[S_σ]**}
D4129	{0.0251**[S_σ]**, -0.2700**[R_σ]**, -0.0121**[R_σ]**}		{-0.0251**[R_σ]**, 0.2700**[S_σ]**, 0.0121**[S_σ]**}
D5127	{0.2039**[S_σ]**, -0.1569**[R_σ]**, -0.0310**[R_σ]**}		{-0.2040**[R_σ]**, 0.1568**[S_σ]**, 0.0311**[S_σ]**}
D5128	{-0.0950**[R_σ]** -0.6328**[R_σ]**, -0.0316**[R_σ]**}		{0.0951**[S_σ]**, 0.6328**[S_σ]**, 0.0316**[S_σ]**}
D5129	{0.9222**[S_σ]**, -0.1541**[R_σ]**, -0.0171**[R_σ]**}		{-0.9222**[R_σ]**, 0.1542**[S_σ]**, 0.0171**[S_σ]**}
E-field = -25×10^{-4} a.u			
D3127	{0.1140**[S_σ]**, -0.4976**[R_σ]**, -0.0644**[R_σ]**}	1.4262**[S_σ, S_σ]**	{-0.1129**[R_σ]**, 0.4976**[S_σ]**, 0.0644**[S_σ]**}
D3128	{0.2034**[S_σ]**, 0.0630**[S_σ]**, -0.0744**[R_σ]**}		{-0.2033**[R_σ]**, -0.0632**[R_σ]**, 0.0747**[S_σ]**}
D3129	{0.6046**[S_σ]**, -0.4883**[R_σ]**, -0.0605**[R_σ]**}		{-0.6046**[R_σ]**, 0.4882**[S_σ]**, 0.0606**[S_σ]**}
D4127	{0.6581**[S_σ]**, -0.5288**[R_σ]**, -0.0470**[R_σ]**}		{-0.6580**[R_σ]**, 0.5288**[S_σ]**, 0.0472**[S_σ]**}
D4128	{0.4036**[S_σ]**, -0.5891**[R_σ]**, -0.0487**[R_σ]**}		{-0.4037**[R_σ]**, 0.5871**[S_σ]**, 0.0485**[S_σ]**}
D4129	{0.1403**[S_σ]**, -0.1480**[R_σ]**, -0.0285**[R_σ]**}		{-0.1401**[R_σ]**, 0.1480**[S_σ]**, 0.0283**[S_σ]**}
D5127	{0.2472**[S_σ]**, -0.0260**[R_σ]**, -0.0549**[R_σ]**}		{-0.2471**[R_σ]**, 0.0259**[S_σ]**, 0.0552**[S_σ]**}
D5128	{0.1974**[S_σ]**, -0.4825**[R_σ]**, -0.0594**[R_σ]**}		{-0.1973**[R_σ]**, 0.4823**[S_σ]**, 0.0595**[S_σ]**}
D5129	{0.3965**[S_σ]**, 0.0769**[S_σ]**, -0.0433**[R_σ]**}		{-0.3965**[R_σ]**, -0.0769**[R_σ]**, 0.0432**[S_σ]**}
E-field = -50×10^{-4} a.u,			
D3127	{0.3633**[S_σ]**, -0.4871**[R_σ]**, -0.0660**[R_σ]**}	1.5676**[S_σ, S_σ]**	{-0.3635**[R_σ]**, 0.4872**[S_σ]**, 0.0662**[S_σ]**}
D3128	{-0.0034**[R_σ]**, 0.2199**[S_σ]**, -0.0763**[R_σ]**}		{0.0036**[S_σ]**, -0.2200**[R_σ]**, 0.0763**[S_σ]**}
D3129	{0.7787**[S_σ]**, -0.1677**[R_σ]**, -0.0580**[R_σ]**}		{-0.7786**[R_σ]**,0.1677**[S_σ]**, 0.0580**[S_σ]**}
D4127	{0.5847**[S_σ]**, 0.0046**[S_σ]**, -0.0498**[R_σ]**}		{-0.5845**[R_σ]**, -0.0048**[R_σ]**, 0.0501**[S_σ]**,
D4128	{0.8954**[S_σ]**, -0.4144**[R_σ]**, -0.0488**[R_σ]**}		{-0.8953**[R_σ]**, 0.4144**[S_σ]**, 0.0489**[S_σ]**}
D4129	{0.2366**[S_σ]**, -0.1085**[R_σ]**, -0.0263**[R_σ]**}		{-0.2367**[R_σ]**, 0.1088**[S_σ]**, 0.0261**[S_σ]**}
D5127	{-0.0381**[R_σ]**, 0.1141**[S_σ]**, -0.0572**[R_σ]**}		{0.0380**[S_σ]**, -0.1140**[R_σ]**, 0.0572**[S_σ]**}
D5128	{-0.1906**[R_σ]**, -0.1132**[R_σ]**, -0.0609**[R_σ]**}		{0.1906**[S_σ]**, 0.1131**[S_σ]**, 0.0607**[S_σ]**}
D5129	{0.6034**[S_σ]**, 0.0392**[S_σ]**, -0.0418**[R_σ]**}		{-0.6035**[R_σ]**, -0.0393**[R_σ]**, 0.0420**[S_σ]**}
E-field = -100×10^{-4} a.u{			
D3127	{0.3460**[S_σ]**, -0.5028**[R_σ]**, -0.0654**[R_σ]**}	1.4209**[S_σ, S_σ]**	{-0.3458**[R_σ]**, 0.5029**[S_σ]**, 0.0655**[S_σ]**}
D3128	{0.0023**[S_σ]**,0.1454**[S_σ]**, -0.0744**[R_σ]**}		{-0.0023**[R_σ]**, -0.1455**[R_σ]**, 0.0744**[S_σ]**}
D3129	{0.7584**[S_σ]**, -0.2316**[R_σ]**, -0.0534**[R_σ]**}		{-0.7583**[R_σ]**, 0.2319**[S_σ]**, 0.0532**[S_σ]**}
D4127	{0.5426**[S_σ]**, -0.0347**[R_σ]**, -0.0510**[R_σ]**}		{-0.5427**[R_σ]**, 0.0346**[S_σ]**, 0.0509**[S_σ]**}
D4128	{0.8704**[S_σ]**, -0.4533**[R_σ]**, -0.0485**[R_σ]**}		{-0.8705**[R_σ]**, 0.4532**[S_σ]**, 0.0484**[S_σ]**}
D4129	{0.1647**[S_σ]**, -0.1257**[R_σ]**, -0.0221**[R_σ]**}		{-0.1648**[R_σ]**, 0.1256**[S_σ]**, 0.0222**[S_σ]**}
D5127	{-0.0464**[R_σ]**, 0.0684**[S_σ]**, -0.0565**[R_σ]**}		{0.0465**[S_σ]**, -0.0683**[R_σ]**, 0.0565**[S_σ]**}
D5128	{-0.1816**[R_σ]**, -0.1650**[R_σ]**, -0.0582**[R_σ]**}		{0.1816**[S_σ]**, 0.1648**[S_σ]**, 0.0582**[S_σ]**}
D5129	{0.5903**[S_σ]**, 0.0365**[S_σ]**, -0.0369**[R_σ]**}		{-0.5903**[R_σ]**, -0.0364**[R_σ]**, 0.0368**[S_σ]**}

4. Supplementary Materials S4. Additional $\mathbb{T}_\sigma(s)$ and tables of the alanine torsional C1-C2 *BCPs.* (continued)

Table S4(b). The values of the chirality $\mathbb{C}_\sigma = [\mathbf{(e_{1\sigma}\cdot dr)_{max}}]_{\mathbf{CCW}} - [\mathbf{(e_{1\sigma}\cdot dr)_{max}}]_{\mathbf{CW}}$, bond-flexing $\mathbb{F}_\sigma = [\mathbf{(e_{2\sigma}\cdot dr)_{max}}]_{\mathbf{CCW}} - [\mathbf{(e_{2\sigma}\cdot dr)_{max}}]_{\mathbf{CW}}$, bond-axiality $\mathbb{A}_\sigma = [\mathbf{(e_{3\sigma}\cdot dr)_{max}}]_{\mathbf{CCW}} - [\mathbf{(e_{3\sigma}\cdot dr)_{max}}]_{\mathbf{CW}}$ and the chirality-helicity function $\mathbb{C}_{helicity} = \mathbb{C}_\sigma|\mathbb{A}_\sigma|$ of the torsional C1-C2 *BCP* of alanine are presented, all entries are multiplied by 10^3.

	S_a		R_a
C1-C2 *BCP*	$\{\mathbb{C}_\sigma, \mathbb{F}_\sigma, \mathbb{A}_\sigma\}$	$\mathbb{C}_{helicity}[\mathbb{C}_\sigma,\|\mathbb{A}_\sigma\|]$	$\{\mathbb{C}_\sigma, \mathbb{F}_\sigma, \mathbb{A}_\sigma\}$
E-field = +25×10^{-4} a.u			
D3127	{0.1875**[S_σ]**, -0.5269**[R_σ]**, -0.0633**[R_σ]**}	1.6074**[S_σ, S_σ]**	{-0.1877**[R_σ]**, 0.5269**[S_σ]**, 0.0635**[S_σ]**}
D3128	{0.1964**[S_σ]**, 0.1349**[S_σ]**, -0.0707**[R_σ]**}		{-0.1964**[R_σ]**, -0.1349**[R_σ]**, 0.0708**[S_σ]**}
D3129	{0.7212**[S_σ]**, -0.4477**[R_σ]**, -0.0633**[R_σ]**}		{-0.7212**[R_σ]**, 0.4478**[S_σ]**, 0.0634**[S_σ]**}
D4127	{0.7072**[S_σ]**, -0.4645**[R_σ]**, -0.0417**[R_σ]**}		{-0.7085**[R_σ]**, 0.4622**[S_σ]**, 0.0411**[S_σ]**}
D4128	{0.5462**[S_σ]**, -0.6080**[R_σ]**, -0.0467**[R_σ]**}		{-0.5459**[R_σ]**, 0.6080**[S_σ]**, 0.0467**[S_σ]**}
D4129	{0.2333**[S_σ]**, -0.1645**[R_σ]**, -0.0313**[R_σ]**}		{-0.2333**[R_σ]**, 0.1646**[S_σ]**, 0.0313**[S_σ]**}
D5127	{0.2064**[S_σ]**, -0.0678**[R_σ]**, -0.0535**[R_σ]**}		{-0.2064**[R_σ]**, 0.0679**[S_σ]**, 0.0534**[S_σ]**}
D5128	{0.1179**[S_σ]**, -0.4227**[R_σ]**, -0.0583**[R_σ]**}		{-0.1177**[R_σ]**, 0.4228**[S_σ]**, 0.0582**[S_σ]**}
D5129	{0.4640**[S_σ]**, 0.0325**[S_σ]**, -0.0468**[R_σ]**}		{-0.4641**[R_σ]**, -0.0325**[R_σ]**, 0.0468**[S_σ]**}
E-field = +50×10^{-4} a.u			
D3127	{0.3842**[S_σ]**, -0.5275**[R_σ]**, -0.0684**[R_σ]**}	1.9453**[S_σ, S_σ]**	{-0.3845**[R_σ]**, 0.5273**[S_σ]**, 0.0683**[S_σ]**}
D3128	{0.0353**[S_σ]**, 0.3194**[S_σ]**, -0.0735**[R_σ]**}		{-0.0354**[R_σ]**, -0.3193**[R_σ]**, 0.0737**[S_σ]**}
D3129	{0.8702**[S_σ]**, -0.1649**[R_σ]**, -0.0683**[R_σ]**}		{-0.8702**[R_σ]**, 0.1649**[S_σ]**, 0.0683**[S_σ]**}
D4127	{0.6954**[S_σ]**, -0.0549**[R_σ]**, -0.0423**[R_σ]**}		{-0.6957**[R_σ]**, 0.0550**[S_σ]**, 0.0425**[S_σ]**}
D4128	{0.9445**[S_σ]**, -0.4437**[R_σ]**, -0.0492**[R_σ]**}		{-0.9445**[R_σ]**, 0.4436**[S_σ]**, 0.0491**[S_σ]**}
D4129	{0.3754**[S_σ]**, -0.1201**[R_σ]**, -0.0353**[R_σ]**}		{-0.3754**[R_σ]**, 0.1201**[S_σ]**, 0.0355**[S_σ]**}
D5127	{0.0031**[S_σ]**, 0.0612**[S_σ]**, -0.0582**[R_σ]**}		{-0.0027**[R_σ]**, -0.0610**[R_σ]**, 0.0583**[S_σ]**}
D5128	{-0.1533**[R_σ]**, -0.1116**[R_σ]**, -0.0625**[R_σ]**}		{0.1533**[S_σ]**, 0.1116**[S_σ]**, 0.0624**[S_σ]**}
D5129	{0.6564**[S_σ]**, 0.0386**[S_σ]**, -0.0528**[R_σ]**}		{-0.6563**[R_σ]**, -0.0387**[R_σ]**, 0.0528**[S_σ]**}
E-field = +100×10^{-4} a.u			
D3127	{0.4430**[S_σ]**, -0.4749**[R_σ]**, -0.0779**[R_σ]**}	2.4307**[S_σ, S_σ]**	{-0.4430**[R_σ]**, 0.4749**[S_σ]**, 0.0780**[S_σ]**}
D3128	{0.0942**[S_σ]**, 0.3688**[S_σ]**, -0.0750**[R_σ]**}		{-0.0942**[R_σ]**, -0.3690**[R_σ]**, 0.0752**[S_σ]**}
D3129	{0.9366**[S_σ]**, -0.0868**[R_σ]**, -0.0786**[R_σ]**}		{-0.9366**[R_σ]**, 0.0867**[S_σ]**, 0.0785**[S_σ]**}
D4127	{0.7467**[S_σ]**, -0.1135**[R_σ]**, -0.0378**[R_σ]**}		{-0.7466**[R_σ]**, 0.1137**[S_σ]**, 0.0379**[S_σ]**}
D4128	{0.9352**[S_σ]**, -0.4556**[R_σ]**, -0.0541**[R_σ]**}		{-0.9351**[R_σ]**, 0.4557**[S_σ]**, 0.0540**[S_σ]**}
D4129	{0.4333**[S_σ]**, -0.0896**[R_σ]**, -0.0438**[R_σ]**}		{-0.4333**[R_σ]**, 0.0895**[S_σ]**, 0.0437**[S_σ]**}
D5127	{0.0956**[S_σ]**, 0.0333**[S_σ]**, -0.0642**[R_σ]**}		{-0.0954**[R_σ]**, -0.0330**[R_σ]**, 0.0643**[S_σ]**}
D5128	{-0.0888**[R_σ]**, -0.1194**[R_σ]**, -0.0687**[R_σ]**}		{0.0887**[S_σ]**, 0.1195**[S_σ]**, 0.0686**[S_σ]**}
D5129	{0.7154**[S_σ]**, 0.0309**[S_σ]**, -0.0638**[R_σ]**}		{-0.7155**[R_σ]**, -0.0310**[R_σ]**, 0.0640**[S_σ]**}